SUBMITTED TO APJ, FEB. 17, 200; RESUBMITTED, NOV. 28, 2000
Preprint typeset using LATEX style emulateapj v. 04/03/99

CONSTRAINTS ON COSMOLOGICAL PARAMETERS FROM FUTURE GALAXY CLUSTER SURVEYS

ZOLTÁN HAIMAN[1,2,3], JOSEPH J. MOHR[4,5,6] & GILBERT P. HOLDER[6]

Submitted to ApJ, Feb. 17, 200; Resubmitted, Nov. 28, 2000

ABSTRACT

We study the expected redshift evolution of galaxy cluster abundance between $0 \lesssim z \lesssim 3$ in different cosmologies, including the effects of the cosmic equation of state parameter $w \equiv p/\rho$. Using the halo mass function obtained in recent large scale numerical simulations, we model the expected cluster yields in a 12 deg^2 Sunyaev-Zel'dovich Effect (SZE) survey and a deep 10^4 deg^2 X-ray survey over a wide range of cosmological parameters. We quantify the statistical differences among cosmologies using both the total number and redshift distribution of clusters. Provided that the local cluster abundance is known to a few percent accuracy, we find only mild degeneracies between w and either Ω_m or h. As a result, both surveys will provide improved constraints on Ω_m and w. The Ω_m–w degeneracy from both surveys is complementary to those found either in studies of CMB anisotropies or of high–redshift Supernovae (SNe). As a result, combining these surveys together with either CMB or SNe studies can reduce the statistical uncertainty on both w and Ω_m to levels below what could be obtained by combining only the latter two data sets. Our results indicate a formal statistical uncertainty of $\approx 3\%$ (68% confidence) on both Ω_m and w when the SZE survey is combined with either the CMB or SN data; the large number of clusters in the X–ray survey further suppresses the degeneracy between w and both Ω_m and h. Systematics and internal evolution of cluster structure at the present pose uncertainties above these levels. We briefly discuss and quantify the relevant systematic errors. By focusing on clusters with measured temperatures in the X–ray survey, we reduce our sensitivity to systematics such as non-standard evolution of internal cluster structure.

Subject headings: cosmology: theory – cosmology: observation

1. INTRODUCTION

It has long been realized that clusters of galaxies provide a uniquely useful probe of the fundamental cosmological parameters. The formation of the large–scale dark matter (DM) potential wells of clusters is likely independent of complex gas dynamical processes, star formation, and feedback, and involve only gravitational physics. As a result, the abundance of clusters $N_{\rm tot}$ and their distribution in redshift dN/dz should be determined purely by the geometry of the universe and the power spectrum of initial density fluctuations. Exploiting this relation, the observed abundance of nearby clusters has been used to constrain the amplitude σ_8 of the power spectrum on cluster scales to an accuracy of $\sim 25\%$ (e.g. White, Efstathiou & Frenk 1993, Viana & Liddle 1996). The value of σ_8 in these studies depends on the assumed underlying cosmology, especially on the density parameters Ω_m and Ω_Λ. Subsequent works (Bahcall & Fan 1998, Blanchard & Bartlett 1998, Viana & Liddle 1999) have shown that the redshift–evolution of the observed cluster abundance places useful constrains on these two cosmological parameters.

In the above studies, the equation of state for the Λ–component has been implicitly assumed to be $p = w\rho$ with $w = -1$. The recent suggestion that w might be different from -1, or even redshift dependent (Turner & White 1997, Caldwell, Dave & Steinhardt 1998) has inspired several studies of cosmologies with a component of dark energy. From a particle physics point of view, such $w > -1$ can arise in a number of theories (see Freese, Adams & Frieman 1987, Ratra & Peebles 1988, Turner & White 1997, Caldwell, Dave & Steinhardt 1998 and references therein). It is therefore of considerable interest to search for possible astrophysical signatures of the equation of state, especially those that distinguish $w = -1$ from $w > -1$. Wang et al. (2000) has summarized current astrophysical constraints that suggest $-1 \leq w \lesssim -0.2$; while recent observations of Type Ia SNe suggest the stronger constraint $w \lesssim -0.6$ (Perlmutter, Turner & White 1999).

The galaxy cluster abundance provides a natural test of models that include a dark energy component with $w \neq -1$, because w directly affects the linear growth of fluctuations D_z, as well as the cosmological volume element $dV/dzd\Omega$. Furthermore, because of the dependence of the angular diameter distance d_A on w, the experimental detection limits for individual clusters, e.g., from the Sunyaev–Zel'dovich effect (SZE) decrement or the X–ray luminosity, depend on w. Wang & Steinhardt (1998, hereafter WS98) studied the constraints on w from a combination of measurements of the cluster abundance and Cosmic Microwave Background (CMB) anisotropies. Their

[1]Hubble Fellow
[2]Princeton University Observatory, Princeton, NJ
[3]NASA/Fermilab Astrophysics Center, Fermi National Accelerator Laboratory, Batavia, IL
[4]Chandra Fellow
[5]Departments of Astronomy and Physics, University of Illinois, 1202 W. Green St, Urbana, IL 61801
[6]Department of Astronomy and Astrophysics, University of Chicago, 5640 S. Ellis Ave, Chicago, IL 60637

work has shown that the slope of the comoving abundance dN/dz between $0 < z < 1$ depends sensitively on w, an effect that can break the degeneracies between w and combinations of other parameters (h, Ω, n) in the CMB anisotropy alone.

Here we consider in greater detail the constraints on w, and other cosmological parameters, from cluster abundance evolution. Our main goals are: (1) to quantify the statistical accuracy to which $w \neq -1$ models can be distinguished from standard Λ Cold Dark Matter (CDM) cosmologies using cluster abundance evolution; (2) to assess these accuracies in two specific cluster surveys: a deep SZE survey (Carlstrom et al. 1999) and a large solid angle X–ray survey, and (3) to contrast constraints from cluster abundance to those from CMB anisotropy measurements and from luminosity distances to high–redshift Supernovae (Schmidt et al. 1998, Perlmutter et al. 1999).

Our work differs from the analysis of WS98 in several ways. We examine the surface density of clusters $dN/dzd\Omega$, rather than the comoving number density $n(z)$. This is important from an observational point of view, because the former, directly measurable quantity inevitably includes the additional cosmology-dependence from the volume element $dV/dzd\Omega$. We incorporate the cosmology–dependent mass–limits expected from both types of surveys. Because the SZE survey has a nearly z–independent sensitivity, we find that high–redshift clusters at $z > 1$ yield useful constraints, in addition to those studied by WS98 in the range $0 < z < 1$. Finally, we quantify the statistical significance of differences in the models by applying a combination of a Kolmogorov–Smirnov (KS) and a Poisson test to $dN/dzd\Omega$, and obtain constraints using a grid of models for a wide range of cosmological parameters.

This paper is organized as follows. In § 2, we describe the main features of the proposed SZE and X-ray surveys relevant to this work. In § 3 we briefly summarize our modeling methods and assumptions. In § 4, we quantify the effect of individual variations of w and of other parameters on cluster abundance and evolution. In § 5, we obtain the constraints on these parameters by considering a grid of different cosmological models. In § 6, we discuss our results and the implications of this work. Finally, in § 7, we summarize our conclusions.

2. CLUSTER SURVEYS

The observational samples available for studies of cluster abundance evolution will improve enormously over the coming decade. The present samples of tens of intermediate redshift clusters (e.g., Gioia et al. 1990, Vikhlinin et al. 1998) will be replaced by samples of thousands of intermediate redshift and hundreds of high redshift ($z > 1$) clusters. At a minimum, the analysis of the European Space Agency *X–ray Multi–mirror Mission (XMM)* archive for serendipitously detected clusters will yield hundreds, and perhaps thousands of new clusters with emission weighted mean temperature measurements (Romer et al. 2000). Dedicated X-ray and SZE surveys could likely surpass the *XMM* sample in areal coverage, number of detected clusters or redshift depth. The imminent improvement of distant cluster data motivates us to estimate the cosmological power of these future surveys. Note that in practice, the only survey details we utilize in our analyses are the virial mass of the least massive, detectable cluster (as a function of redshift and cosmological parameters), and the solid angle of the survey. We include here a brief description of two representative surveys.

2.1. *A Sunyaev–Zel'dovich Effect Survey*

The SZE survey we consider is that proposed by Carlstrom and collaborators (Carlstrom et al. 1999). This interferometric survey is particularly promising, because it will detect clusters more massive than $\sim 2 \times 10^{14} M_\odot$, nearly independent of their redshift. Combined, this low mass threshold and its redshift independence produce a cluster sample which extends, depending on cosmology, to redshifts $z \sim 3$. The proposed survey will cover 12 deg^2 in a year; it will be carried out using ten 2.5 m telescopes and an 8 GHz bandwidth digital correlator operating at cm wavelengths (Mohr et al. 1999). The detection limit as a function of redshift and cosmology $M_{\min}(z, \Omega_m, h)$ for this survey has been studied using mock observations of simulated galaxy clusters (Holder et al. 2000), and we draw on those results here.

Optical and near infrared followup observations will be required to determine the redshifts of SZE clusters. Given the relatively small solid angle of the survey, it will be straightforward to obtain deep, multiband imaging. We expect that the spectroscopic followup will require access to a multiobject spectrograph on a 10 m class telescope. The ongoing development of infrared spectrographs may greatly enhance our ability to effectively measure redshifts for the most distant clusters detected in the SZE survey.

2.2. *A Deep, Large Solid Angle X–ray Survey*

We also consider the cosmological sensitivity of a large solid angle, deep X-ray imaging survey. The characteristics of our survey are similar to those of a proposed Small Explorer class mission, called the Cosmology Explorer, spear-headed by G. Ricker and D. Lamb. The survey depth is 3.6×10^6 cm^{2}s at 1.5 keV, and the coverage is 10^4 deg^2 (approximately half the available unobscured sky). We assume that the imaging characteristics of the survey are sufficient to allow separation of the 10% clusters from the 90% AGNs and galactic stars. We focus on clusters which produce 500 detected source counts in the 0.5:6.0 keV band, sufficient to reliably estimate the emission weighted mean temperature in a survey of this depth (the external and internal backgrounds sum to ~ 1.4 cts/arcmin^2).

To compute the number of photons detected from a cluster of a particular flux, we assume the clusters emit Raymond–Smith spectra (Raymond & Smith 1977) with $\frac{1}{3}$ solar abundance, and we model the effects of Galactic absorption using a constant column density of $n_H = 4 \times 10^{20}$ cm^{-2}. The metallicity and Galactic absorption we've chosen are representative for a cluster studied in regions of high Galactic latitude; when analyzing a real cluster one would, of course, use the Galactic n_H appropriate at the location of the cluster. Cluster metallicities vary, but for the 0.5:6 keV band, line emission contributes very little flux for clusters with temperatures above 2 keV. For example, if the cluster metallicity were doubled to $\frac{2}{3}$ solar, the conversion between flux and the observed counts in the 0.5:6 keV band for this particular survey would vary by $\sim 1.4\%$ and $\sim 0.1\%$ for Raymond-Smith spectral models with temperatures $kT = 2$ keV and 10 keV, respectively. We assume that the detectors have a quantum efficiency similar to the ACIS detectors (Bautz et al. 1998, Chartas et al. 1998) on the *Chandra X-ray Observatory*, and the energy dependence of the mirror effective area mimics that of the mirror modules on ABRIXAS (Friedrich et al. 1998).

The X-ray survey could be combined with the Sloan Digital Sky Survey (SDSS) to obtain redshifts for the clusters – the redshift distribution of the clusters which produce 500 photons in the survey described above is well sampled at the SDSS photometric redshift limit.

2.3. *Determining the Survey Limiting Mass $M_{\rm min}$*

For our analysis, the most important aspect of both surveys is the limiting halo mass $M_{\rm min}(z, \Omega_m, w, h)$, as a function of redshift and cosmological parameters. More specifically, we seek the relation between the detection limit of the survey, and the corresponding limiting "virial mass". In our modeling below, we will be using the mass function of dark halos obtained in large scale cosmological simulations (Jenkins et al. 2000). In these simulations, halos are identified as those regions whose mean spherical overdensity exceeds the fixed value $\delta\rho/\rho_b = 180$ (with respect to the background density ρ_b, and irrespective of cosmology; see discussion below). In what follows, we adopt the same definition for the mass of dark halos associated with galaxy clusters.

In the X-ray survey, $M_{\rm min}$ follows from the cluster X-ray luminosity – virial mass relation and the details of the survey. We adopt the relation between virial mass and temperature obtained in hydrodynamical simulations by Bryan & Norman (1998),

$$M_{\rm vir} = a\frac{T^{3/2}}{E(z)\sqrt{\Delta_c(z)}}, \qquad (1)$$

where $H(z) = H_0 E(z)$ is the Hubble parameter at redshift z, $a = 1.08$ is a normalization determined from the hydrodynamical simulations, and Δ_c is the enclosed overdensity (relative to the critical density) which defines the cluster virial region. The normalization a is found to be relatively insensitive to cosmological parameters, and the redshift evolution of Equation 1 appears to be consistent with the hydrodynamical simulations in those models where it has been tested (Bryan & Norman 1998). Here we assume that Equation 1 holds in all cosmologies with the same value of a (see §6.2 for a discussion of the effects of errors in the mass-temperature relation), and use the fitting formulae for Δ_c provided by WS98, which includes the case $w \neq -1$. Finally, we convert $M_{\rm vir}$ from Equation 1 to the mass M_{180} enclosed within the spherical overdensity of $\delta\rho/\rho = 180$ (with respect to the background density), assuming that the halo profile is well described by the NFW model with concentration $c = 5$ (Navarro, Frenk & White 1997, hereafter NFW).

We next utilize Equation 1, together with the relation between bolometric luminosity and temperature found by Arnaud & Evrard (1999), to find the limiting mass of a cluster that produces 500 photons in the 0.5:6.0 keV band in a survey exposure. For these calculations we assume that the luminosity-temperature relation does not evolve with redshift, consistent with the currently available observations (Mushotzky & Scharf 1997; relaxing this assumption is discussed below in § 6).

For an interferometric SZE survey, the relevant observable is the cluster visibility V, which is the Fourier transform of the cluster SZE brightness distribution on the sky as seen by the interferometer. The visibility is proportional to the total SZE flux decrement S_ν,

$$V \propto S_\nu(M,z) \propto f_{ICM}\frac{M\langle T_e\rangle_n}{d_A^2(z)} \qquad (2)$$

where $\langle T_e\rangle_n$ is the electron density weighted mean temperature, M is the virial mass, f_{ICM} is the intracluster medium mass fraction and d_A is the angular diameter distance. We normalize this relation using mock observations of numerical cluster simulations (see Mohr & Evrard 1997 and Mohr, Mathiesen & Evrard 1999) carried out in three different cosmological models, including noise characteristics appropriate to the proposed SZE array (see Holder et al. 2000 for more details). The ICM mass fraction is set to $f_{ICM} = 0.12$ in all three cosmological models. This mass fraction is consistent with analyses of X-ray emission from well defined samples if $H_0 = 65$ km s^{-1} Mpc^{-1}, our fiducial value. Note that we use the same $f_{ICM} = 0.12$ in all our cosmological models rather than varying it with the H_0 scaling appropriate for analyses of cluster X-ray emission. In the discussion which follows, this choice allows us to focus solely on the cosmological discriminatory power of cluster surveys; naturally, in interpreting a real cluster survey one would likely allow f_{ICM} to vary with H_0.

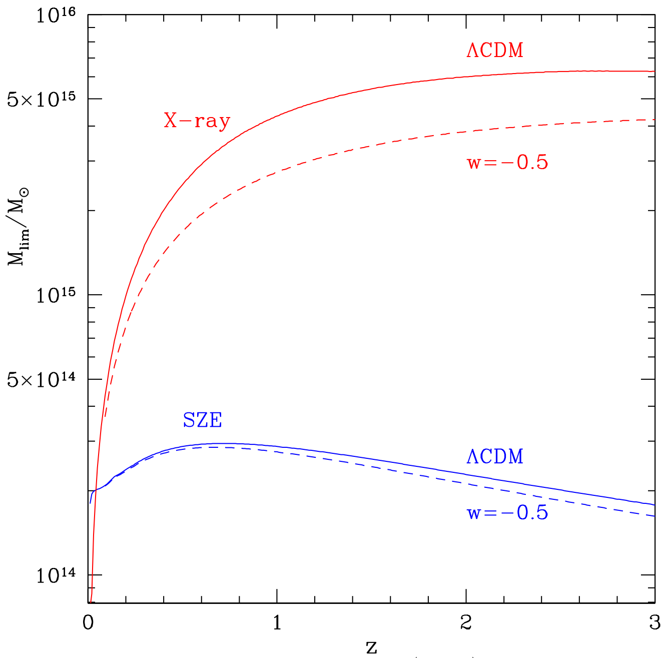

FIG. 1.— Limiting cluster virial masses (M_{180}) for detection in the X-ray survey (upper pair of curves) and in the SZE survey (lower pair of curves). The solid curves show the mass limit in our fiducial flat ΛCDM model, with $w = -1$, $\Omega_m = 0.3$, and $h = 0.65$, and the dotted curves show the masses in the same model except with $w = -0.5$.

Note that for a flux limited survey, the limiting mass in equation 2 is sensitive to cosmology through its dependence on d_A and the definition of the virial mass M. We adopt the simulation–normalized value of $M^*_{\rm min}(z)$ in our fiducial cosmology as a template, and then we rescale this relation to determine $M_{\min}(z)$ in the model of interest using the relation

$$M_{\min}(z) = M^*_{min}(z)\frac{h^*}{h}\left[\frac{hd_A(z)}{h^*d^*_A(z)}\right]^{6/5} \tag{3}$$

Here the superscript * refers to quantities in the ΛCDM reference cosmology, and we have used the scaling of virial mass with temperature (Eqn. 1): $M \propto \langle T_e\rangle_n^{3/2}$. We tested this scaling by comparing it to mock observations in simulations of two different cosmologies (open CDM and standard CDM), and found that agreement was better than $\sim 10\%$ in the redshift range $0 < z < 3$. Finally, in the numerical simulations used to calibrate Equation 2, the halo mass was defined to be the total mass enclosed within a region whose mean spherical interior density is 200 times the critical density. As in the X–ray case, we convert $M_{\min}(z)$ from Equation 3 to the desired mass M_{180} by assuming that the halo profile follows NFW with concentration $c = 5$.

The mass limits we derive for both surveys are shown in the redshift range $0 < z < 3$ in Figure 1, both for ΛCDM and for a $w = -0.5$ universe. The SZE mass limit is nearly independent of redshift, and changes little with cosmology. As a result, the cluster sample can extend to $z \approx 3$. In comparison, the X–ray mass limit is a stronger function of w, and it rises rapidly with redshift. For the X-ray survey considered here the number of detected clusters beyond $z \approx 1$ is negligible.

These mass limits incorporate some simplifying assumptions that have not been tested in detail (although we consider small variations of the mass limits below). Our goal is to capture the scaling with cosmological parameters and redshift as best as presently possible. However, we emphasize that further theoretical studies of the sensitivities of these scalings to, for example, energy injection during galaxy formation will be critical to interpreting the survey data. In the case of the X–ray survey, the cluster sample will have measured temperatures, allowing the limiting mass to be estimated independent of the cluster luminosity. In the case of the SZE survey, deep X-ray followup or multifrequency SZE followup observations should yield direct measurements of the limiting mass.

3. ESTIMATING THE CLUSTER SURVEY YIELD

To derive cosmological constraints from the observed number and redshift distribution of galaxy clusters, the fundamental quantity we need to predict is the comoving cluster mass function. The Press–Schechter formalism (Press & Schechter 1974; hereafter PS), which directly predicts this quantity in any cosmology, has been shown to be in reasonably good agreement (i.e. to within a factor of two) with results of N–body simulations, in cosmologies and halo mass ranges where it has been tested (Lacey & Cole 1994, Gross et al 1998, Lee & Shandarin 1999). Numerical simulations have only recently reached the large size required to accurately determine the mass function of the rarest, most massive objects, such as galaxy clusters with $M > 10^{15}M_\odot$.

In this paper, we adopt the halo mass function found in a series of recent large–scale cosmological simulations by Jenkins et al. 2000. The results of these simulations are particularly well–suited for the present application. The large simulated volumes allow a statistically accurate determination of the halo mass function; for halo masses of interest here, to better than $\lesssim 30\%$. In addition, the mass function is computed in three different cosmologies at a range of redshifts, and found to obey a simple 'universal' fitting formula. Although this does not guarantee that the same scaling holds in other, untested cosmologies, we make this simplifying assumption in the present paper. In the future, the validity of this assumption has to be tested by studying the numerical mass function across a wider range of cosmologies.

Generally, the simulation mass function predicts a significantly larger abundance of massive clusters than does the PS formula. For sake of definiteness, we note that in the simulations, halos are identified as those regions whose mean spherical overdensity exceeds the fixed value $\delta\rho/\rho_b = 180$ with respect to the background density ρ_b. This is somewhat different from the typical halo definition within the context of the PS formalism, where the overdensity, relative to the critical density, is taken to be that of a collapsing spherical top–hat at virialization.

Following Jenkins et al. 2000, we assume that the comoving number density $(dn/dM)dM$ of clusters at redshift z with mass $M \pm dM/2$ is given by the formula,

$$\frac{dn}{dM}(z,M) = 0.315\frac{\rho_0}{M}\frac{1}{\sigma_M}\frac{d\sigma_M}{dM}\exp\left[-\left|0.61 - \log(D_z\sigma_M)\right|^{3.8}\right], \tag{4}$$

where σ_M is the r.m.s. density fluctuation, computed on mass–scale M from the present–day linear power spectrum (Eisenstein & Hu 1998), D_z is the linear growth function, and ρ_0 is the present–day mass density. The directly observable quantity, i.e. the average number of clusters with mass above $M_{\min}$ at redshift $z \pm dz/2$ observed in a solid angle $d\Omega$ is then simply given by

$$\frac{dN}{dzd\Omega}(z) = \left[\frac{dV}{dzd\Omega}(z)\int_{M_{\min}(z)}^{\infty} dM\frac{dn}{dM}\right] \tag{5}$$

where $dV/dzd\Omega$ is the cosmological volume element, and $M_{\min}(z)$ is the limiting mass as discussed in section 2.3. Equations 4 and 5 depend on the cosmological parameters through ρ_0, D_z, and $dV/dzd\Omega$, in addition to the mild dependence of σ_M on these parameters through the power spectrum (although the dependence on the power–spectrum is more pronounced in the X–ray survey, where the limiting mass varies strongly with redshift). Note that the comoving abundance dn/dM is exponentially sensitive to the growth function D_z. We use convenient expresions for $dV/dzd\Omega$ and D_z in open and flat Ω_Λ cosmologies available in the literature (Peebles 1980, Carroll, Press & Turner 1992, Eisenstein 1996). In the case of cosmologies with $w \neq -1$, we have evaluated $dV/dzd\Omega$ numerically, but used the fitting formulae for D_z obtained by WS98, which are accurate to better than 0.3% for the cases of constant w's considered here.

3.1. *Normalizing to Local Cluster Abundance*

To compute $dN/dzd\Omega$ from equation 5, we must choose a normalization for the density fluctuations σ_M. This is commonly expressed by σ_8; the present epoch, linearly extrapolated *rms* variation in the density field filtered on scales of $8h^{-1}$ Mpc. To be consistent in our analysis, we choose the normalization for each cosmology by fixing the local cluster abundance above a given mass $M_{\rm nm} = 10^{14}h^{-1}\ M_\odot$. In all models considered, we set the local abundance to be $1.03 \times 10^{-5}\ (h/0.65)^3\ {\rm Mpc}^{-3}$, the value derived in our fiducial ΛCDM model (see below). We have chosen to normalize using the local cluster abundance (upto a factor h^3) above mass $M_{\rm nm}$ rather than above a particular emission weighted mean temperature $kT_{\rm nm}$, because this removes the somewhat uncertain cosmological sensitivity of the virial mass temperature ($M-T_x$) relation from the normalization process; spherical tophat calculations suggest a significant offset in the $M-T_x$ normalization of the open and flat $\Omega_m = 0.3$ models which hydrodynamical simulations do not seem to reproduce (Evrard, Metzler & Navarro 1996, Bryan & Norman 1998, Viana & Liddle 1999).

An alternative approach to the above is to regard σ_8 a "free–parameter", on equal footing with the other parameters we let float below. This possibility will be discussed further in § 6. Here we note that our normalization approach is sensible, because the number density of nearby clusters can be measured to within a factor of h^3, and the masses of nearby clusters can be measured directly through several independent means; these include the assumption of hydrostatic equilibrium and using X-ray images and intracluster medium (ICM) temperature profiles, weak lensing, or galaxy dynamical mass estimates. The only cosmological sensitivity of these mass estimators is their dependence on the Hubble parameter h; we include this h dependence when normalizing our cosmological models. Note that previous derivations of σ_8 (e.g. Viana & Liddle 1993; Pen 1998) in various cosmologies from the local cluster abundance $N(>kT)$ above a fixed threshold temperature $kT_{\rm min} \sim 7$keV yielded a constraint with the approximate scaling $\sigma_8\Omega_m^{1/2} \approx 0.5$. We find a similar relation when varying Ω_m away from our fiducial cosmology; however, we note that if a $\sim$ 5 times smaller threshold temperature were used, the constrained combination would be quite different, $\sigma_8\Omega_m$ ∼constant. Since our adopted normalization is based on mass, rather than temperature, in general, we find still different scalings. As an example, when $h = 0.65$ and $w = -1$ are kept fixed, our normalization procedure translates into $\sigma_8(\Omega_m/0.3)^{0.85} \approx 0.9$.

3.2. *Fiducial Cosmological Model*

The parameters we choose for of our fiducial cosmological model are $(\Omega_\Lambda, \Omega_{\rm m}, h, \sigma_8, n) = (0.7, 0.3, 0.65, 0.9, 1)$. This flat ΛCDM model is motivated as a "best–fit" model that produces a local cluster abundance consistent with observations (Viana & Liddle 1999), and satisfies the current constraints from CMB anisotropy (Lange et al. 2000, see also White, Scott & Pierpaoli 2000), high–z SNe, and other observations (Bahcall et al. 1999). We have assumed a baryon density of $\Omega_b h^2 = 0.02$, consistent with recent D/H measurements (e.g. Burles & Tytler 1998). Note that the power spectrum index n is not important for the analysis presented here, because we normalize on cluster scales σ_8, and we find that this minimizes the effect of varying n on the density fluctuations relevant to cluster formation.

4. EXPLORING THE COSMOLOGICAL SENSITIVITY

In this section, we describe how variations of the individual parameters Ω, w, and h, as well as the cosmological dependence of the limiting mass $M_{\rm min}$, affect the cluster abundance and redshift distribution. This will be useful in understanding the results of the next section, when a full grid of different cosmologies is considered. We then describe our method of quantifying the statistical significance of differences between the distributions dN/dz in a pair of different cosmologies.

4.1. *Single Parameter Variations*

The surface density of clusters more massive than $M_{\rm min}$ depends on the assumed cosmology mainly through the growth function $D(z)$ and volume element $dV/dzd\Omega$, as well as through the cosmology–dependence of the limiting mass $M_{\rm min}$ itself. In the approach described in section 3, once a cosmology is specified, the normalization of the power spectrum σ_8 is found by keeping the abundance of clusters at $z = 0$ constant. We therefore consider only three "free" parameters, w, h, Ω_m, specifying the cosmology. We assume the universe to be either flat ($\Omega_Q = 1 - \Omega_m$), or open with $\Omega_Q = 0$.

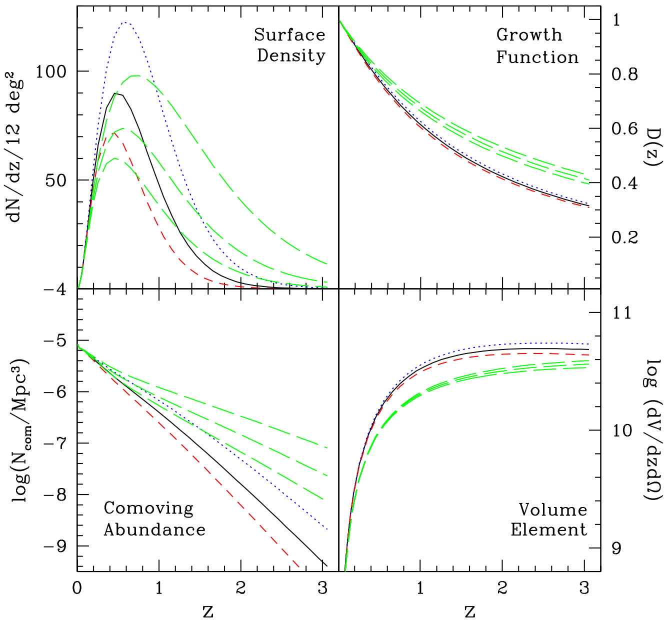

FIG. 2.— Effect of changing Ω_m when all other parameters are held fixed. The four panels show (clockwise from upper left) the surface density of clusters at redshift z; the linear growth function; the volume element in units of ${\rm Mpc}^3\ {\rm sr}^{-1}$ redshift^{-1}; and the comoving cluster abundance. The solid curve shows our fiducial flat ΛCDM model, with $w = -1$, $\Omega_m = 0.3$, and $h = 0.65$. Also shown are models with $\Omega = 0.27$ (dotted curve); $\Omega = 0.33$ (short–dashed curve); and OCDM models with $\Omega = 0.27, 0.30, 0.33$ (long–dashed curves, top to bottom).

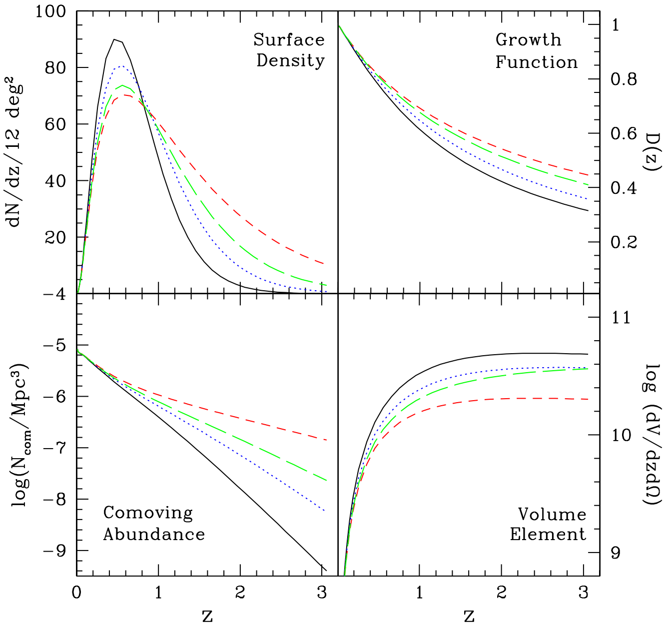

FIG. 3.— Effect of changing w when all other parameters are held fixed. The solid curve shows our fiducial flat ΛCDM model, with $w = -1$, $\Omega_m = 0.3$, and $h = 0.65$. The dotted curve is the same model with $w = -0.6$, the short–dashed curve with $w = -0.2$, and the long–dashed curve is an open CDM model with $\Omega_m = 0.3$.

4.1.1. *Changing* Ω_m

The effects of changing Ω_m are demonstrated in Figure 2. The curves correspond to a flat ΛCDM universe with $(h = 0.65, w = -1)$, and $\Omega_m = 0.27$ (dotted), $\Omega_m = 0.30$ (solid), and $\Omega_m = 0.33$ (short–dashed). In addition, the long–dashed curves show the same three models (top to bottom), assuming open CDM with $\Omega_\Lambda = 0$. The top left panel shows the total number of clusters in a 12 square degree field, detectable down to the constant SZE decrement $S_{\rm min}$. As discussed in section 2.3 above, a constant $S_{\rm min}$ implies a redshift and cosmology–dependent limiting mass $M_{\rm min}$. In the SZE case, we find that if we had not included this effect, the sensitivity to Ω_m would have been somewhat stronger. Several conclusions can be drawn from Figure 2. Overall, the top left panel shows that a decrease in Ω_m increases the number of clusters (and vice versa) at all redshifts. Note that the dependence is strong, for instance, a 10% decrease in Ω_m increases the total number of clusters by $\sim$ 30% in either ΛCDM or OCDM cosmologies. As emphasized by Bahcall & Fan (1998), Viana & Liddle (1999) and others, this makes it possible to estimate an upper limit on Ω_m using current, sparse data on cluster abundances (i.e. only a few high–z clusters). A second important feature seen in the top left panel is that the shape of the redshift distribution is not changed significantly, a conclusion that holds both in ΛCDM and OCDM. Finally, the remaining three panels reveal that the effects of Ω_m arise mainly from the changes in the comoving abundance (bottom left panel). In flat ΛCDM, Ω_m has relatively little effect on the volume or the growth function, and the comoving abundance is determined by the value of σ_8 that keeps the the local abundance constant at $z = 0$ (we find σ_8=0.83 for $\Omega_m = 0.33$ and $\sigma_8 = 1.00$ for $\Omega_m = 0.27$). In addition, we find that the change in the shape of the underlying power spectrum with Ω_m enhances the differences caused by Ω_m (when we artificially keep the power spectrum at its $\Omega_m = 0.3$ shape, we find σ_8=0.84 for $\Omega_m = 0.33$). We also note that the volume element and the comoving abundance act in the same direction: a lower Ω_m increases both the comoving abundance and the volume element. In OCDM, the growth function has a larger effect, and relative to ΛCDM, the redshift distribution is much flatter.

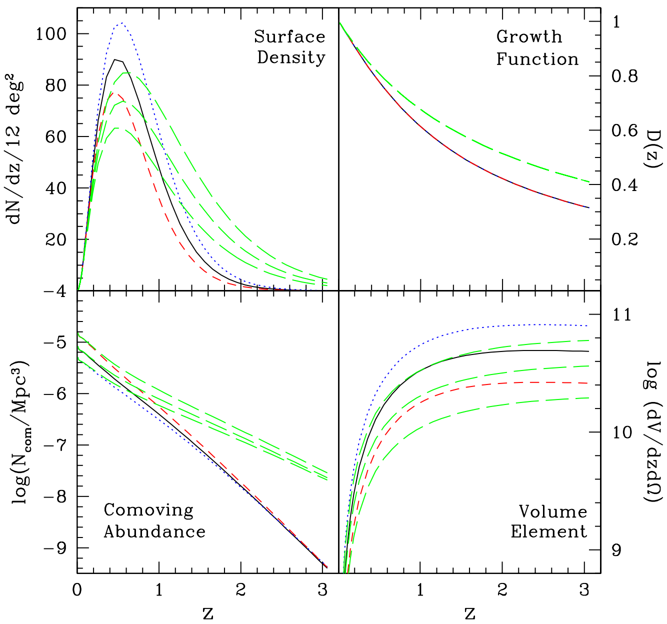

FIG. 4.— Effect of changing h when all other parameters are held fixed. The ΛCDM model of Figure 3 is shown (solid curve) together with models with $h = 0.55$ (dotted curve); $h = 0.80$ (short–dashed curve); and OCDM models with $h = 0.55, 0.65, 0.80$ (long–dashed curves, top to bottom).

4.1.2. *Changing* w

The effects of changing w are demonstrated in Figure 3. The figure shows models with $(\Omega_m = 0.3, h = 0.65)$ and with three different w's: $w = -1$ (solid curve), $w = -0.6$ (dotted curve), and $w = -0.2$ (short–dashed curve). In addition, we show the result from an open CDM model with $(\Omega = 0.3, h = 0.65$; long–dashed curve). The figure reveals that increasing w above $w = -1$ causes the slope of the redshift distribution above $z \approx 0.5$ to flatten, increasing the number of high–z clusters. Furthermore, "opening" the universe has an effect similar to increasing w. The other three panels demonstrate the reason for these scalings. The top right panel shows that the growth function is flatter in higher w models, significantly increasing the comoving number density of high–redshift clusters (bottom left panel). The volume element (bottom right panel) has the opposite behavior, in the sense the volume in higher–w models is smaller, which tends to balance the increase in the comoving abundance caused by the growth function in the range $0 < z \lesssim 0.5$; but for higher redshifts, the growth function "wins". An important conclusion seen from Figure 3 is that both the total number of clusters as well as the shape of their redshift distribution, significantly depends on w. We also note that in the SZE case, our sensitivity to w has been enhanced by the cosmological dependence of the mass limit (opposite to what we found for the Ω_m–sensitivity, which we found was weakened by the same effect).

4.1.3. *Changing h*

Figure 4 demonstrates the effects of changing h. Three ΛCDM models are shown with $(\Omega_m = 0.30, w = -1)$, and $h = 0.55$ (dotted curve), $h = 0.65$ (solid curve), and $h = 0.80$ (short–dashed curves). The long–dashed curves correspond to OCDM models with the same parameters (top to bottom). Comparing the top right panel with that of Figure 2, the qualitative behavior of dN/dz under changes in h and Ω_m are similar: decreasing h increases the total number of clusters, but does not considerably change their redshift distribution. However, the sensitivity to h is significantly less: the total number of clusters is seen to increase by $\sim 25\%$ only when h is decreased by the same percentage. Note that the growth function is not effected by h, and the h sensitivity is driven by our normalization process, which fixes the abundance at $z = 0$ (see § 3.1). Since the volume scales as $\propto h^{-3}$, we fix the comoving abundance to be proportional to $\propto h^3$. As a result, $dN/dzd\Omega$ is nearly independent of h. In fact, the entire h–dependence is attributable to the small change caused by h in the shape of the power spectrum (for a pure power–law spectrum, there would be no h–dependence, and the three curves for the flat universe in the top left panel of Figure 4 would look identical).

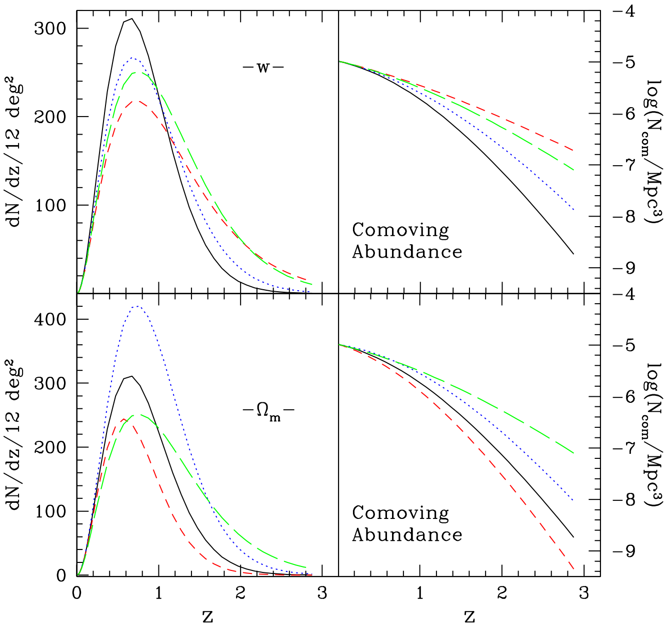

FIG. 5.— Effect of changing w (upper panels) or Ω_m (lower panels) when all other parameters are held fixed, including the mass limit. The types of the curves correspond to the different models in the SZE survey, as shown in Figures 2 & 3.

4.1.4. *Abundances in the X–ray Survey*

The evolution of the cluster abundance, and its sensitivity to Ω_m and w in the X–ray survey are shown in Figure 6. Because of the much larger solid angle surveyed, the numbers of clusters is significantly larger than in the SZE case, despite the higher limiting mass (cf. Fig 1). Nevertheless, the general trends that can be identified in the X–ray sample are similar to those in the SZE case. Raising w increases the total number of clusters, and flattens their redshift distribution. As in the SZE survey, raising Ω_m decreases the total number of clusters.

4.2. *Effects of the Limiting Mass Function*

Finally, we examine the extent to which the above conclusions depend on the cosmology and redshift–dependence of the limiting mass $M_{\rm min}$.

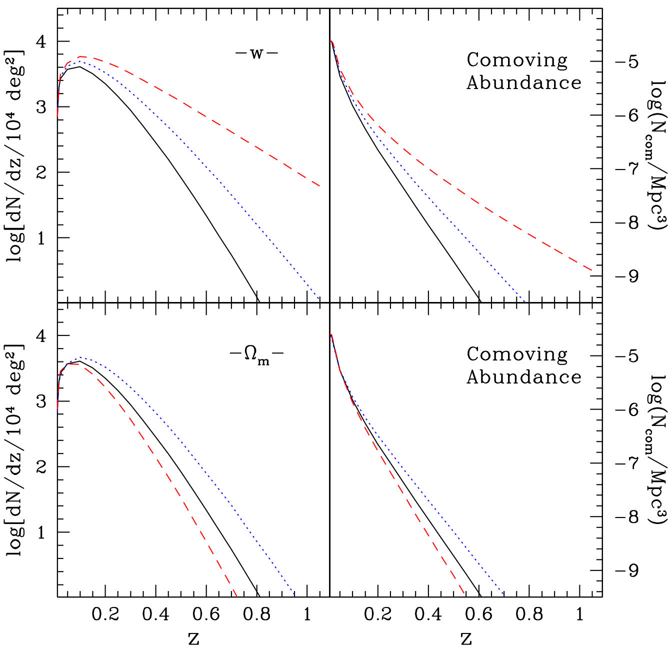

FIG. 6.— Effect of changing w (upper panels) or Ω_m (lower panels) when all other parameters are held fixed in the X–ray survey. Note the much larger numbers of clusters in comparison to the SZE survey. In the top panel, the curves correspond to $w = -1$ (solid), $w = -0.6$ (dotted) and $w = -0.2$ (dashed). In the bottom panel, the curves correspond to $\Omega_m = 0.3$ (solid), $\Omega_m = 0.27$ (dotted) and $\Omega_m = 0.33$ (dashed).

4.2.1. *The SZE Survey*

We first compute cluster abundances above the fixed mass $M_{\rm min} = 10^{14}h^{-1}{\rm M}_\odot$, characteristic of the SZE survey detection threshold in the range of cosmologies and redshifts considered here. The results are shown in Figure 5: the bottom panels show the surface density and comoving abundance when Ω_m is changed (the models are the same as in Figure 2), and the top panels show the same quantities under changes in w (the cosmological models are the same as in Figure 3). A comparison between Figures 5 and 3 gives an idea of the importance of the mass limit. The general trend seen in Figure 3 remains true, i.e. increasing w flattens the redshift distribution at high–z. However, when a constant $M_{\rm min}$ is assumed, the "pivot point" moves to slightly higher redshift, and the total number of clusters becomes less sensitive to w. Similar conclusions can be drawn from a comparison of Figure 2 with the bottom two panels of Figure 5: under changes in Ω_m the general trends are once again similar, but the differences between the different models are amplified when a constant $M_{\rm min}$ is used. In summary, we conclude that in the SZE case (1) the variation of the mass limit with redshift and cosmology has a secondary importance, and (2) it weakens the Ω_m dependence, but strengthens the w dependence.

4.2.2. *The X–ray Survey*

In comparison to the SZE survey, the X–ray mass limit is not only higher, but is also significantly more dependent on cosmology (cf. Fig 1). On the other hand, the X–ray sample goes out only to the relatively low redshift $z = 1$, where the growth functions in the different cosmologies diverge relatively little. This suggests that in the X–ray case the mass limit is more important than in the SZE survey. In order to separate the effects of the changing mass limit from the change in the growth function and the volume element, in Figure 7 we show the sensitivity of dN/dz to changes in Ω_m and w, without including the effects from the mass limit. The same models are shown as in Figure 6, except we have artificially kept the mass limit at its value in the fiducial cosmology. The figure reveals that essentially all of the w–sensitivity seen in Figure 6 is caused by the changing mass limit; when $M_{\rm min}$ is kept fixed, the cluster abundances change very little. On the other hand, comparing the bottom panels of Figures 6 and 7 shows that including the scaling of the mass limit somewhat reduces the Ω_m dependence, just as in the SZE case.

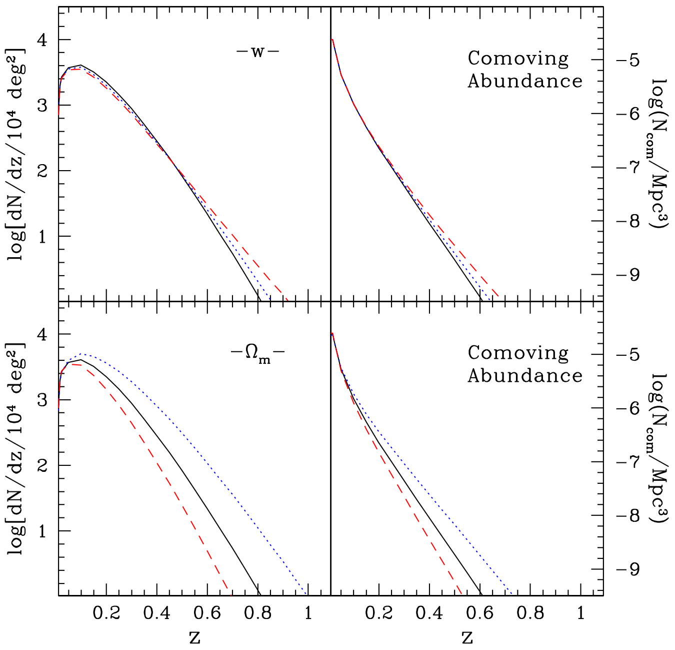

FIG. 7.— Effect of changing w (upper panels) or Ω_m (lower panels) when all other parameters are held fixed in an X–ray survey, and the survey mass limit is held fixed at its fiducial value, irrespective of cosmology. A comparison with Figure 6 shows that nearly all of the w–sensitivity is accounted for by the cosmology–dependence of the limiting mass. On the other hand, the Ω_m–sensitivity is caused mostly by the growth function.

4.3. *Overview of Cosmological Sensitivity*

In summary, we conclude that changes in w modify both the normalization and the shape of the redshift distribution of clusters, while changes in Ω_m or h effect essentially only the overall amplitude. This suggests that changes in w can not be fully degenerate with changes in either Ω_m or h (or a combination), making it possible to measure w from cluster abundances alone. These conclusions hold either for clusters above a fixed detection threshold in and SZE or X-ray survey, or for a sample of clusters above a fixed mass. We find that the sensitivity to Ω_m arises mostly through the growth function, both in the SZE and X–ray surveys. This sensitivity is slightly weakened by the scaling of the limiting mass $M_{\rm min}$ with Ω_m. We find that the w sensitivity is also dominated by the growth function in the SZE survey, which goes out to relatively high redshifts; but the sensitivity to w is enhanced by the w–dependence of $M_{\rm min}$. In comparison, in the X–ray survey, which only probes relatively low redshifts, nearly all of the w–sensitivity is caused by the cosmology–dependence of the limiting mass, rather than the growth function.

5. CONSTRAINTS ON COSMOLOGICAL PARAMETERS

We derive cosmological constraints by considering a 3–dimensional grid of models in Ω_m, h, and w. As described above, we first find σ_8 in each model, so that all models are normalized to produce the same local cluster abundance at $z = 0$. We then compute $dN/dzd\Omega$ in these models for $0.2 \leq \Omega_m \leq 0.5$, $0.5 \leq h \leq 0.9$, and $-1 \leq w \leq -0.2$. The range for w corresponds to that allowed by current astrophysical observations (Wang et al. 2000); although recent observations of Type Ia SNe suggest the stronger constraint $w \lesssim -0.6$ (Perlmutter, Turner & White 1999).

5.1. *Comparing dN/dz in Two Different Cosmologies*

The main goal of this paper is to quantify the accuracy to which w can be measured in future SZE and X–ray surveys. To do this, we must answer the following question: given a hypothetical sample of $N_{\rm tot}$ clusters (with measured redshifts) obeying the distribution dN_A/dz of the test model (A) cosmology, what is the probability $P_{\rm tot}(A,B)$ that the same sample of clusters is detected in the fiducial (B) cosmology, with distribution dN_B/dz? We have seen in section 4.1 that the overall amplitude, and the shape of dN/dz are both important. Motivated by this, we define

$$P_{\rm tot}(A,B) = P_0(A,B) \times P_z(A,B) \qquad (6)$$

where $P_0(A,B)$ is the probability of detecting $N_{A,\rm tot}$ clusters when the mean number is $N_{B,\rm tot}$, and $P_z(A,B)$ is the probability of measuring the redshift distribution of model (A) if the true parent distribution is that of model (B). We assume P_0 is given by the Poisson distribution, and we use the Kolmogorov–Smirnov (KS) test to compute $P_z(A,B)$ (Press et al. 1992). The main advantage of this approach, when compared to the usual χ^2 tests, is that we do not need to bin the data in redshift.

For reference, it is useful to quote here some examples for the probabilities, taking $(\Omega_m = 0.3, h = 0.65, w = -1)$ as the fiducial (B) model. For example, closest to this model in Figure 3 is the one with $w = -0.6$. For this case, we find $P_0 = 0.25$ and $P_z = 0.1$ for a total probability of $P_{\rm tot} = 0.025$. In other words, the two cosmologies could be distinguished at a likelihood of 1.2σ using only the total number of clusters, at 1.6σ using only the shape of the redshift distribution, and at the 2.3σ level using both pieces of information. In this case, the distinction is made primarily by the different redshift distributions, rather than the total number of detected clusters. Taking the $\Omega_m = 0.33$ ΛCDM cosmology from Figure 2 as another example for model (A), we find $P_0 = 0.0075$ (=2.7σ), $P_z = 0.78$ (=0.3σ), and a total probability of

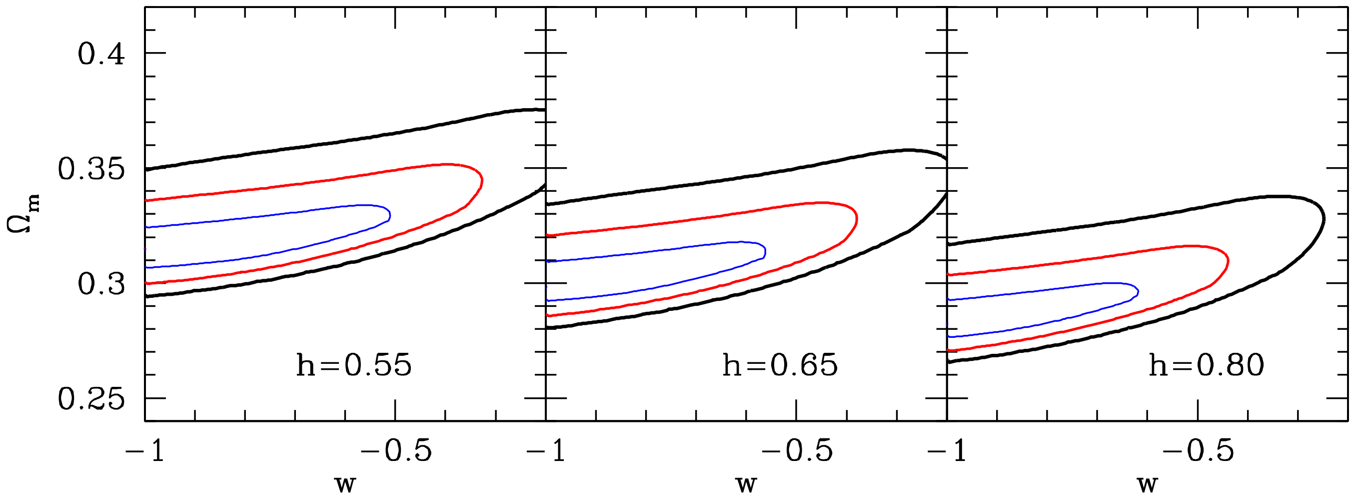

FIG. 8.— Contours of 1, 2, and 3σ likelihood for different models when they are compared to a fiducial flat ΛCDM model with $\Omega_m = 0.3$ and $h = 0.65$, using the SZE survey. The three panels show three different cross–sections of constant total probability at fixed values of h (0.55,0.65, and 0.80) in the investigated 3–dimensional Ω_m, w, h parameter space.

$P_{\rm tot} = 0.0058$ (=2.8σ). Not surprisingly, the shape of the redshift distribution does not add significantly to the statistical difference between these two models, which differ primarily by the total number of clusters.

5.2. *Expectations from the Sunyaev–Zel'dovich Survey*

Figure 8 shows contours of 1, 2, and 3σ for the total probability $P_{\rm tot}$ for models when compared to the fiducial flat ΛCDM model. For reference, we note that the total number of clusters in the SZE survey in our fiducial model is ≈ 100, located between $0 < z < 3$. The three panels show three different cross–sections of the investigated 3–dimensional Ω_m, h, w parameter space, taken at constant values of $h = 0.55$, 0.65, and 0.80, spanning the range of values preferred by other observations. The most striking feature in this figure is the direction of the contours, which turn upwards in the w, Ω_m plane, and become narrower for larger values of w. We find that the trough of maximum probability for fixed $h = 0.65$ is well described by

$$(\Omega_m - 0.3)(w+1)^{-5/2} = 0.1, \qquad (7)$$

with further constant shifts in Ω_m caused by changing h. The $\pm 3\sigma$ width enclosed by the contours around this relation is relatively narrow in Ω_m ($\pm 10\%$). In a ΛCDM case, even when a large range of values is considered for h ($0.45 < h < 0.90$), the constraint $0.26 \lesssim \Omega_m \lesssim 0.36$ follows; when $w \neq -1$ is considered, the allowed range widens to $0.27 \lesssim \Omega_m \lesssim 0.41$. On the other hand, a wide range of w's is seen to be consistent with $w = -1$: the largest value shown, $w \approx -0.2$ is approximately 3σ away from $w = -1$, and $w = -0.6$ is allowed at 1σ. Note that h is not well determined, i.e. the contours look similar for all three values of h, and 1σ models exist for any value of h in the range $0.5 \lesssim h \lesssim 0.9$. This is not surprising, as Figure 4 shows $dN/dzd\Omega$ is insensitive to the value of h, with only a mild h–dependence through the non–power law shape of the power spectrum.

5.3. *Expectations from the X–ray Survey*

The total number of clusters in the X–ray survey in our fiducial model is ≈ 1000, ten times that in the SZE survey; all X–ray clusters are located between $0 < z < 1$.

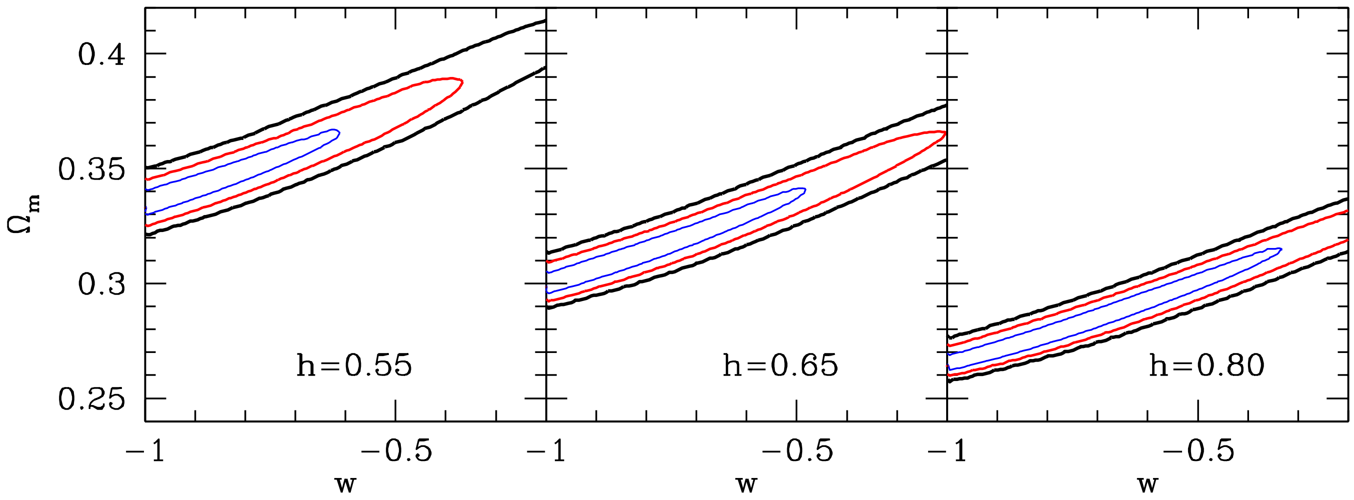

FIG. 9.— Contours of 1, 2, and 3σ likelihood for models when they are compared to a fiducial flat ΛCDM model, as in Figure 8, but for the X–ray survey.

Figure 9 contains expectations for the X-ray survey; we show contours of 1, 2, and 3σ probabilities relative to the fiducial ΛCDM model. The qualitative features are similar to that in the SZE case, but owing to the larger number of clusters, the constraints are significantly stronger and the contours are narrower. However, the contours extend further along the w axis, and the largest value of w allowed at a probability better than 3σ is $w > -0.2$ (assuming that the values of Ω_m and h are not known). Although the contours are narrower than in the SZE case, assuming that h and w are unknown, the allowed range of Ω_m is similar to that in the SZE case, $0.26 \lesssim \Omega_m \lesssim 0.42$. Note that because of the shape and direction of the likelihood contours, a knowledge of h would not significantly improve this constraint (although if h is found to be low, then the lower limit in Ω_m would increase). Finally, assuming that both h and Ω_m are known to high accuracy ($\approx 3\%$), the allowed 3σ range on w could be reduced to $-1 \leq w \lesssim -0.85$.

6. RESULTS AND DISCUSSION

6.1. *Total Number vs. the Redshift Distribution*

Our main results are presented in Figures 8 and 9, which show the probabilities of various models relative to a fiducial ΛCDM model in the SZE and X-ray surveys. As demonstrated by these figures, the cluster data determine a combination of Ω_m and w. In the absence of external constraints on Ω_m and h, w as large as -0.2 differs from $w = -1$ by 3σ; while $w = -0.6$ would be 1σ away from our fiducial ΛCDM cosmology. Owing to the larger number of clusters in the X–ray survey, the constrained combination of Ω_m and w is significantly narrower than in the SZE survey; the direction of the contours is also somewhat different. As a result, analysis of the X–ray survey could distinguish a $w \approx -0.85$ model from ΛCDM at 3σ significance, provided Ω_m is known to an accuracy of $\sim 3\%$ from other studies.

It is interesting to ask whether these constraints arise mainly from the total number of detected clusters, or from their redshift distribution. To address this issue, in Figure 10 we show separate likelihood contours for the probability P_0 (total number of clusters, left panels), and for the probability P_z (shape of redshift distribution, right panels). In the SZE case, the contours of likelihood from the shape information alone are broad, and adding these constraints to the Poisson–probability plays almost no role in the range $w \lesssim -0.7$ (the contours of $P_{\rm tot}$ and P_0 are very similar). However, at larger w, the shape becomes increasingly important. Adding in this information significantly reduces the allowed region relative to the Poisson–probability alone at $w \gtrsim -0.7$. It is the combination of the P_0 and P_z contours that allows ruling out $w \gtrsim -0.2$ at the 3σ level. Note that the difference in shapes arises mostly from the high–redshift ($z \gtrsim 1$) clusters (cf. Fig. 3).

In the X–ray case (bottom panels in Fig. 10), the situation is different, because the contours of P_0 and P_z are both much narrower. As a result, the contours for the combined likelihood are somewhat reduced, but they still reach to $w \approx -0.2$ (at $\sim 2\sigma$). Note that as in the SZE survey, the redshift distribution (of clusters primarily in the $0 < z < 1$ range) plays an important role. As Figures 4 and 2 show, the total number of clusters can be adjusted by changing Ω_m and h. In terms of the total number of clusters, w is therefore degenerate both with Ω_m and h: raising w lowers the total number, but this can always be offset by a change in Ω_m and/or h. The bottom left panel in Fig. 10 reveals that based on P_0 alone, $w = -0.2$ (and $\Omega_m = 0.43$) can not be distinguished from ΛCDM even at the 1σ level. On the other hand, the middle panel in Fig. 9 shows that when the shape information is added, $w \lesssim -0.2$ follows to 2σ significance.

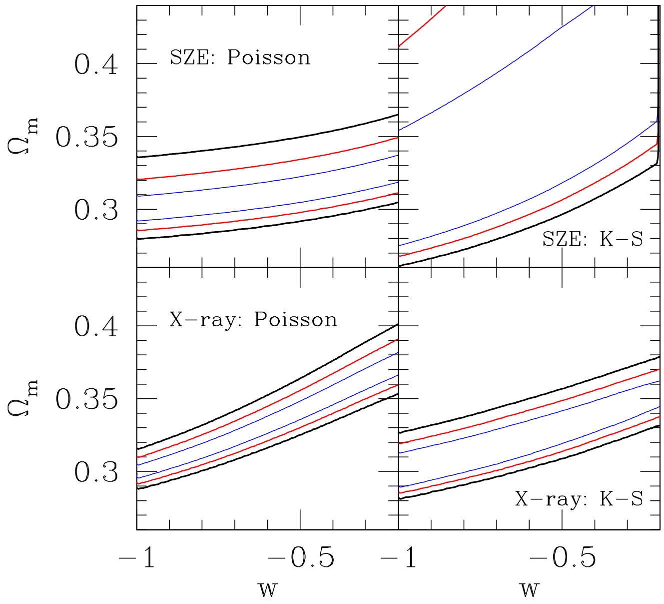

FIG. 10.— Likelihood contours of 1, 2, and 3σ probabilites as in Figures 8 and 9, but when only the total number of clusters (left panels), or only the redshift distributions (right panels) are used to compute the likelihoods between two models.

6.2. *Discussion of Possible Systematic Uncertainties*

Our results imply that the cluster abundances in the SZE and X–ray surveys can provide useful constraints on cosmological parameters, based on statistical differences expected among different cosmologies. The purpose of this section is to summarize and quantify the various systematic uncertainties that can affect these constraints.

Knowledge of the Limiting Mass $M_{\rm min}$. Our conclusions above are dependent on the chosen limiting mass, which is a function of both redshift and cosmology. From the discussion in § 4.1 we have seen that the limiting mass plays a secondary role in the SZE survey, where the bulk of the constraint comes from the growth function. In comparison, we find that $M_{\rm min}$ plays an important role in the X–ray survey. To demonstrate the importance of the mass limit explicitly, in Figure 11 we show the likelihood contours in the $\Omega_m - w$ plane when the variations of the limiting mass with cosmology are not taken into account. Not surprisingly, this makes the contours somewhat narrower, but nearly parallel to w – this is consistent with our finding in Figure 7 that the mass limit accounts for nearly all of the w–dependence, but it reduces the Ω_m dependence. Figure 11 demonstrates the need to accurately know the limiting mass $M_{\rm min}$, and its cosmological scaling, in the X–ray survey.

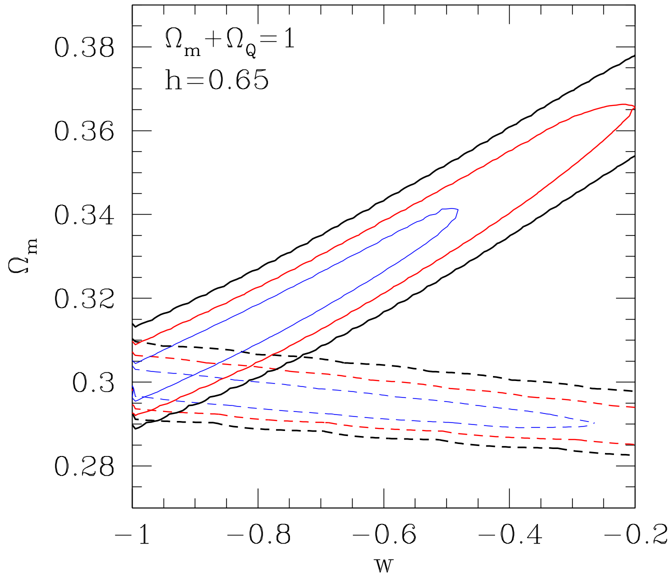

FIG. 11.— Likelihood contours for a fixed $h = 0.65$ in the X–ray survey, as in the middle panel of Figure 9, but zooming in for clarity. The added (nearly horizontal) contours shows the allowed region when variations of the limiting mass with cosmology are not taken into account.

Because our proposed cluster sample will have measured X–ray temperatures, the uncertainty in our knowledge of the limiting mass will likely be dominated by the theoretical uncertainties of the $M-T$ relation. In order to quantify the effect of such errors, we have performed a set of simple modifications to our modeling of the constraints from the X–ray survey. In all cases, we adopt the same $M-T$ relations as we did before (cf. eq. 1). However, in the fiducial model, we use a limiting mass that is altered by either $\pm5\%$ or $\pm10\%$ from the mass inferred from this $M-T$ relation. This mimics a situation where the theoretical $M-T$ relation we apply is either 5% or 10% away from the relation in the real universe. In a second set of calculations, we mimic a situation where the slope of the $M-T$ relation is incorrectly modeled; i.e. we alter this slope in the fiducial model to $\alpha = 1.5 \pm 0.05$. The deviations to the likelihood contours caused by these offsets are demonstrated in Figure 12, which shows the effects of the offset in the $M-T$ normalization, and in Figure 13, which shows the effects of the offsets in the slope. As the figures reveal, the contours shift relatively little under these changes. We conclude that the results we derive are robust, as long as we can predict the $M-T$ relation to within $\sim 10\%$.

In our approach, we have attempted to utilize the whole observed cluster sample, down to the detection threshold: we had to therefore include the above cosmological dependencies. In principle, measured cluster velocity dispersions and X–ray temperatures (both of which are cosmology independent) could be utilized to improve the constraints, i.e. by selecting sub–samples that maximize the differences between models. Further work is needed to clarify the feasibility of this approach, as well as to quantify the accuracy to which the dependence of $M_{\rm min}$ on Ω_m, h, w, and z can be predicted.

Evolution of Internal Cluster Structure. Further work is also required to test the cluster structural evolution models we use. For the X–ray survey, we have assumed that the cluster luminosity–temperature relation does not evolve, consistent with current observations (Mushotzky & Scharf 1997), and in the SZE survey, we have adopted the structural evolution found in state of the art hydrodynamical simulations. Because of the sensitivity of the survey yields to the limiting mass, cluster structural evolution which changes the observability of high redshift clusters can introduce systematic errors in cosmological constraints: for example, both low Ω_m cosmologies and positive evolution of the cluster luminosity–temperature relation increase the cluster yield in an X-ray survey. SZE surveys are generally less sensitive to evolution than X–ray surveys, because the X–ray luminosity is heavily dependent on the core structure (e.g., the presence or absence of cooling instabilities), whereas the SZE visibility depends on the integral of the ICM pressure over the entire cluster (Eqn. 2). We are testing these assertions with a new suite of hydrodynamical simulations in scenarios where galaxy formation at high redshift preheats the intergalactic gas before it collapses to form clusters (Bialek, Evrard & Mohr 2000; Mohr et al. in prep). However, most importantly, we emphasize that because of the sensitivity of X–ray surveys to evolution, we have only used those clusters which produce enough photons to measure an emission weighted mean temperature. In this case, one can directly extract the minimum temperature $T_{lim}(z)$ of detected clusters as a function of redshift. Correctly interpreting such a survey requires mapping $T_{lim}(z) \rightarrow M_{lim}(z)$ using the mass-temperature relation; the evolution of the mass-temperature relation is less sensitive to the details of preheating than the luminosity-temperature relation. Thus, in a survey constructed in this manner, it should be possible to disentangle the cosmological effects from those caused by the evolution of cluster structure.

Cluster Mass Function. In our treatment, we have relied on the mass function inferred from large scale numerical simulations of Jenkins et al. (2000). Although we do not expect the results presented here to change qualitatively, changes in dN/dM by upto the quoted accuracy of $\sim 30\%$ could affect the exact shape of the likelihood contours shown in Figures 8 and 9. It is important to test the scaling of the mass function with cosmological parameters in future simulations. We have further ignored the effects of galaxy formation and feedback on the limiting mass. In principle, the relation between the cluster SZE decrement and virial mass in the lowest mass clusters could be affected by these processes. In addition, the dependence of both the SZE decrement and the X–ray flux likely exhibits a non–negligible intrinsic scatter. The SZE decrement to virial mass relation is found to have a small scatter in numerical simulations (Metzler 1998), and to cause a negligible increase in the total cluster yields (Holder et al. 1999). However, the presence of scatter could effectively lower the limiting masses in our treatment of the X–ray survey.

Local Cluster Abundance. Perhaps the most critical assumption is that the local cluster abundance is known to high accuracy. We have used this assumption to determine σ_8, i.e. to eliminate one free parameter – effectively assign-

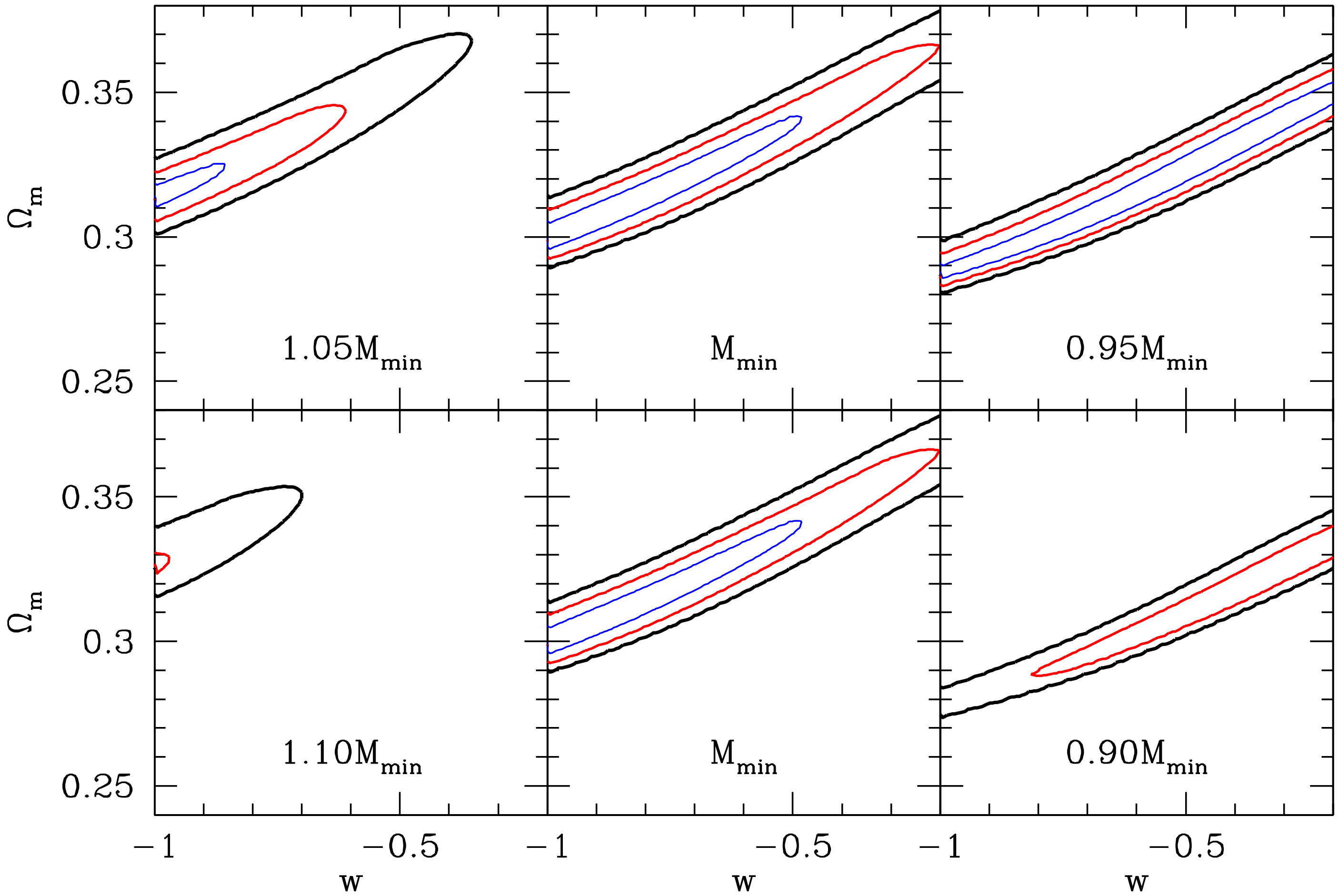

FIG. 12.— The middle panels show the likelihood contours for a fixed $h = 0.65$ in the X–ray survey, as in Figure 9. The upper and lower panels show the deviations in the contours caused by either a ±5% or a ±10% offset in the $M - T$ normalization.

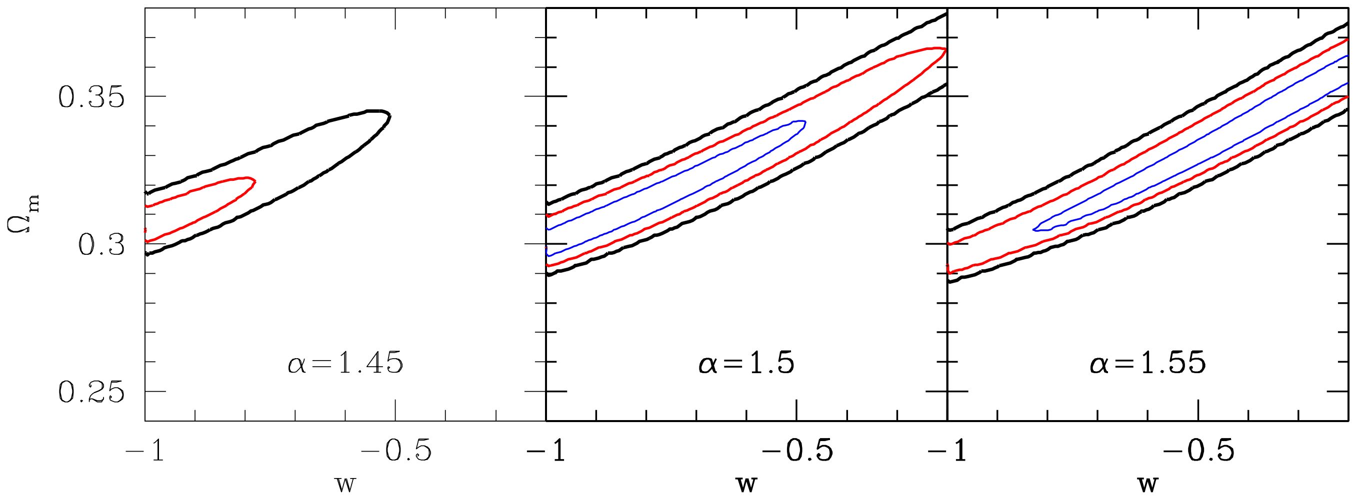

FIG. 13.— The middle panels show the likelihood contours for a fixed $h = 0.65$ in the X–ray survey, as in Figure 9. The other two panels show the deviations caused by an offset in the slope $M \propto T^{\alpha}$.

ing "infinite weight" to the cluster abundance near $z = 0$. This approach is appropriate for several reasons. The cosmological parameters make little difference to the cluster abundance at $z \approx 0$, other than the volume being proportional to h^{-3}. Similarly, the study of local cluster masses is cosmologically independent (upto a factor of h). In a 10^4 square degree survey, we find that the total number of clusters between $0 < z < 0.1$, down to a limiting mass of $2 \times 10^{14} h^{-1}$ M$_{\odot}$ is ≈ 2500; with a random error of only ±2%. We have experimented with our models, assuming that the normalization at $z = 0$ is incorrectly determined by a fraction of 2%. In Figure 14, we show the shift in the usual likelihood contour in the X–ray survey, caused by errors in the local abundance at this level. As the figure shows, the shift is relatively small (by about the width of the 1σ region). In similar calculations with errors of ±4%, we find shifts that are approximately twice as significant. We conclude that for our normalization procedure to be valid, the local cluster abundance has to be known to an accuracy of about $\lesssim 10\%$.

Although such an accuracy can be achieved by only ~ 600 nearby clusters (which can be provided, for example, by an analysis of the SDSS data or perhaps the 2MASS survey), it is interesting to consider a different approach, where σ_8 is treated as another free parameter in addition to Ω_m, h, and w. The result of such a calculation over a 4–dimensional grid is displayed in Figure 15. This figure shows the likelihood contours along the slice $h = 0.65$ through this parameter space, but in projection along the σ_8 axis; to be compared directly with the middle panel of Figure 9. Allowing σ_8 to vary results in a range of values $0.70 < \sigma_8 < 0.97$, and considerably expands the allowed likelihood region. The shape of the contours stay nearly unchanged, but their widths along the Ω_m direction expand by approximately a factor of ~ 4, and their lengths along the w direction increase by about a factor of 2. We conclude that our constraints would be significantly weakened without the local normalization (but would still be potentially useful when combined with other data; see below).

More General Cosmologies. In section 5, we restricted our range of models to flat CDM models. We find that the redshift distribution of clusters in open CDM models typically resembles that in models with high w. This is demonstrated in Figure 3: both in the $w = -0.2$ and the OCDM model, the redshift distributions are flatter and extend to higher z than in ΛCDM. We find that OCDM models with suitably adjusted values of Ω_m and h are typically difficult to distinguish from those with $w \gtrsim -0.5$, but the flat shape of $dN/dzd\Omega$ makes OCDM easily distinguishable from ΛCDM. Note that open CDM models appear inconsistent with the recent CMB anisotropy data from the Boomerang and Maxima experiments (e.g. Lange et al. 2000, White, Scott & Pierpaoli 2000, Bond et al. 2000). A broader study of different cosmological models, including those with both dark energy and curvature, time–dependent w, and those with non–Gaussian initial conditions could reveal new degeneracies, and will be studied elsewhere.

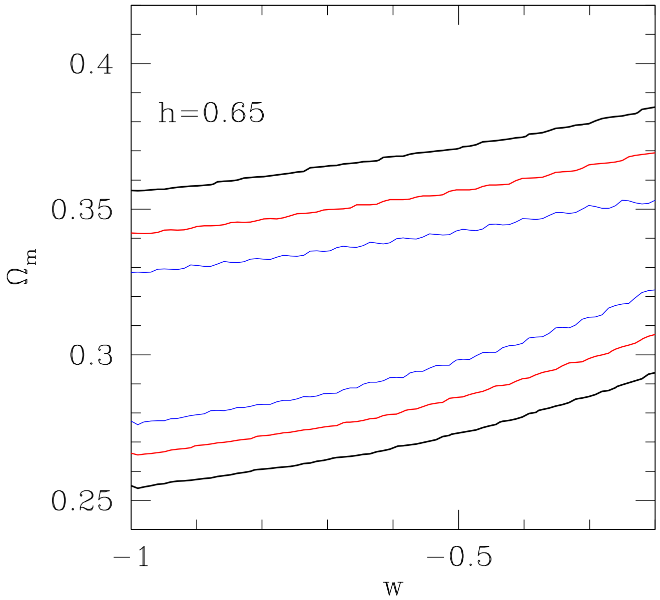

FIG. 15.— Likelihood contours for a fixed $h = 0.65$ in the X–ray survey, as in Figure 9; however, we here considered σ_8 as a free parameter, rather than fixing its value based on the local abundance. For the range of Ω and w shown, models with a likelihood better than 3σ take on values between $0.7 < \sigma_8 < 0.97$.

6.3. *Clusters versus CMB Anisotropy and High-z SNe*

A useful generic feature of the likelihood contours presented here is their difference from those expected in CMB anisotropy or Supernovae data. Two different cosmologies produce the same location (spherical harmonic index $\ell_{\rm peak}$) for the first Doppler peak for the CMB temperature anisotropy, provided they have the same comoving distance to the surface of last scattering (cf. Wang & Steinhardt 1998, White 1998, Huey et al. 1999). Note that this is only the most prominent constraint that can be obtained from the CMB data, with considerable more information once the location and height of the second and higher Doppler peaks are measured. Similarly; the appar-

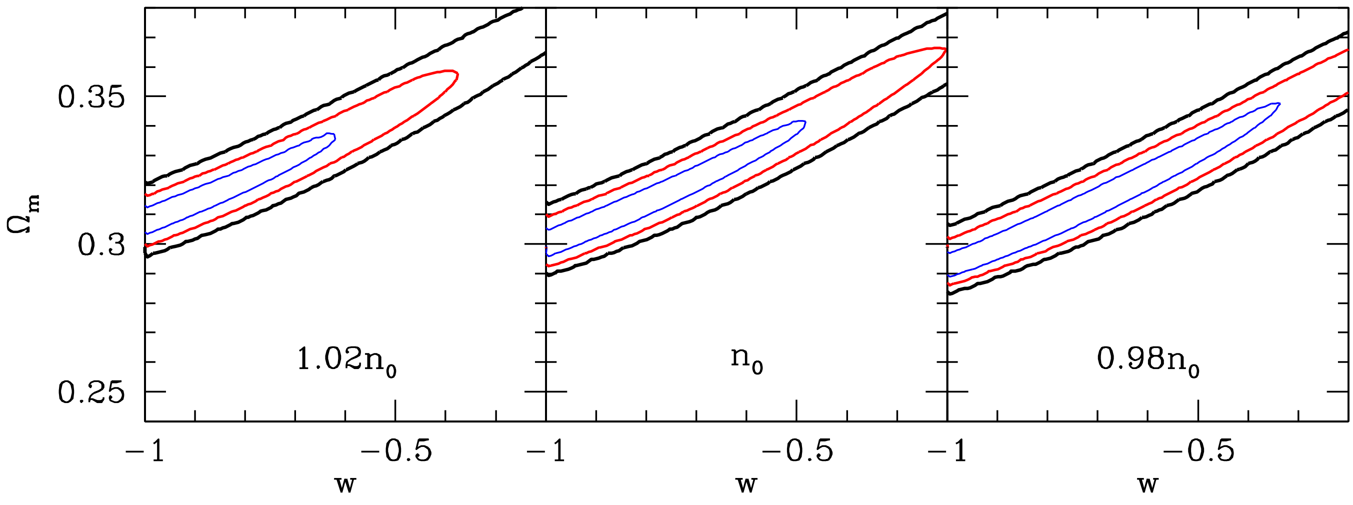

FIG. 14.— The middle panel shows the likelihood contours for a fixed $h = 0.65$ in the X–ray survey, as in Figure 9. The left and right panels show the deviations in the contours caused by a $\pm 2\%$ offset in the local cluster abundance determination.

ent magnitudes of the observed SNe constrain the luminosity distance $d_L(z)$ to $0 \leq z \lesssim 1$ (Schmidt et al. 1998, Perlmutter et al. 1999). In general, both of these types of observations will determine a combination of cosmological parameters that is different from the cluster constraints derived here.

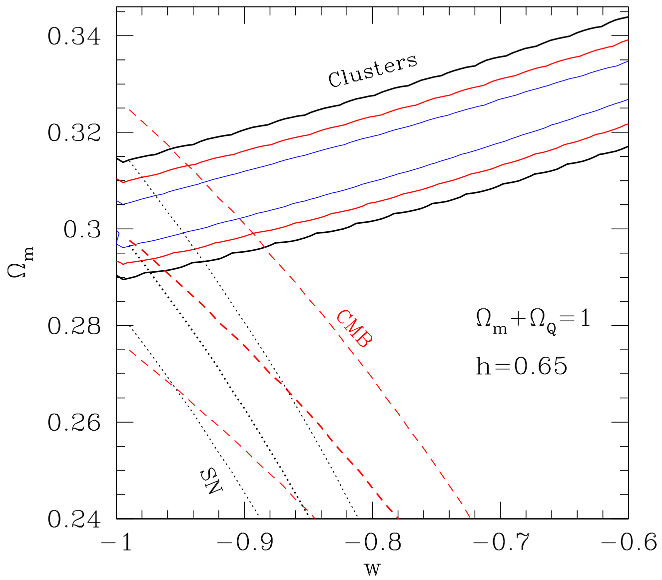

FIG. 16.— Likelihood contours for a fixed $h = 0.65$ as in Figure 9, but zooming in for clarity. Also shown are combinations of w and Ω_m that keep the spherical harmonic index ℓ of the first Doppler peak in the CMB anisotropy data constant to within $\pm1\%$ (dashed lines); and combinations that keep the luminosity distance to redshift $z = 1$ constant to the same accuracy.

In Figure 16, we zoom in on the relevant region of the $\Omega_m - w$ plane in the X–ray survey, and compare the cluster constraints to those expected from CMB anisotropy or high–z SNe. The three dashed curves correspond to the CMB constraints: the middle curve shows a combination of Ω_m and w that produces the constant $\ell_{\rm peak} \approx 243$ obtained in our fiducial ΛCDM model (using the fitting formulae from White 1998 for the physical scale $k_{\rm peak}$); the other two dotted curves bracket a $\pm1\%$ range around this value. Similarly, the dotted curves correspond to the constraints from SNe. The middle curve shows a line of constant d_L at $z = 1$ that agrees with the ΛCDM model; the two other curves produce a d_L that differs from the fiducial value by $\pm1\%$. As the figures show, the lines of CMB and SNe parameter degeneracies run somewhat unfavorably parallel to each other; however, both of those degeneracies are much more complementary to the direction of the parameter degeneracy in cluster abundance studies. In particular, the maximum allowed value of w, using both the CMB or SNe data, is $w \approx -0.8$; while this is reduced to $w \approx -0.95$ when the cluster constraints are added. Note that in Figure 16, we have assumed a fixed value of $h = 0.65$; however, we find that relaxing this assumption does not significantly change the above conclusion. The CMB and SNe constraints depend more sensitively on h than the cluster constraints do: as a result, the confidence regions do not overlap significantly even in the three–dimensional (w, Ω_m, h) space.

The high complementarity of the cluster constraint to those from the other two methods can be understood based on the discussions in § 4.1. To remain consistent with the CMB and SNe Ia constraints, an increase in w must be coupled with a decrease in Ω_m; however, both increasing w and lowering Ω_m raises the number of detected clusters. To keep the total number of clusters constant, an increase in w must be balanced by an increase in Ω_m. Note that this statement is true both for the SZE and the X–ray surveys. Combining the cluster constraints with the CMB and SNe Ia constraints will therefore likely result in improved estimates of the cosmological parameters, and we do not expect this conclusion to rely on the details of the two surveys considered here.

7. CONCLUSIONS

We studied the expected evolution of galaxy cluster abundance from $0 \lesssim z \lesssim 3$ in different cosmologies, including the effects of variations in the cosmic equation of state parameter $w \equiv p/\rho$. By considering a range of cosmological models, we quantified the accuracy to which Ω_m, w, and h can be determined in the future, using a 12 deg^2 Sunyaev-Zel'dovich Effect survey and a deep 10^4 deg^2 X-ray survey. In our analysis, we have assumed that the local cluster abundance is known accurately: we find that in practice, an accuracy of $\sim 5\%$ is sufficient for our results to be valid.

We find that raising w significantly flattens the redshift–distribution, which can not be mimicked by variations in either Ω_m, h, which affect essentially only the normalization of the redshift distribution. As a result, both surveys will be able to improve present constraints on w. In the $\Omega_m - w$ plane, both the SZE and X–ray surveys yield constraints that are highly complementary to those obtained from the CMB anisotropy and high–z SNe. Note that the SZE and X–ray surveys are themselves somewhat complementary. In combination with these data, the SZE survey can determine both w and Ω_m to an accuracy of $\approx 10\%$ at 3σ significance. Further improvements will be possible from the X–ray survey. The large number of clusters further alleviates the degeneracy between w and both Ω_m and h, and, as a result, the X–ray sample can determine w to $\approx 10\%$ and Ω_m to $\approx 5\%$ accuracy, in combination with either the CMB or the SN data.

Our work focuses primarily on the statistics of cluster surveys. We have provided an estimate of the scale of various systematic uncertainties. Further work is needed to clarify the role of these uncertainties, arising especially from the analytic estimates of the scaling of the mass limits with cosmology, the dependence of the cluster mass function on cosmology, and our neglect of issues such as galaxy formation in the lowest mass clusters. However, our findings suggest that, in a flat universe, the cluster data lead to tight constraints on a combination of Ω_m and w, especially valuable because of their high complementarity to those obtained from the CMB anisotropy or Hubble diagrams using SNe as standard candles.

We thank L. Hui for useful discussions, D. Eisenstein, M. Turner, D. Spergel and the anonymous referee for useful comments, and J. Carlstrom and the COSMEX team for providing access to instrument characteristics required to estimate the yields from their planned surveys. ZH is supported by the DOE and the NASA grant NAG 5-7092 at Fermilab, and by NASA through the Hubble Fellowship grant HF-01119.01-99A, awarded by the Space Telescope Science Institute, which is operated by the Association of Universities for Research in Astronomy, Inc., for NASA under contract NAS 5-26555. JJM is supported by Chandra Fellowship grant PF8-1003, awarded through the Chandra Science Center. The Chandra Science Center is operated by the Smithsonian Astrophysical Observatory for NASA under contract NAS8-39073.

REFERENCES

Arnaud, M. & Evrard, A.E. 1999, MNRAS, 305, 631
Bahcall, N.A., Ostriker, J. P., Perlmutter, S., & Steinhardt, P. J. 1999, Science, 284, 1481
Bahcall, N.A. & Fan, X. 1998, ApJ, 504, 1
Bautz, M.W., Pivovaroff, M., Baganoff, G., Isobe, T., Jones, S.E., Kissel, S.E., Lamarr, B., Manning, H.L., Prigozhin, G.Y., Ricker, G.R., Nousek, J.A., Grant, C.E., Nishikida, D., Scholze, F., Thornagel, R., & Ulm, G. 1998, SPIE Proceeding, 3444, 210
Bialek, J., Evrard, A.E. & Mohr, J.J. 2000, ApJ, submitted (astro-ph/0010584)
Blanchard, A. & Bartlett, J.G. 1998, A&A, 332, L49
Bond, J. R., & Myers, S. T. 1996, ApJS, 103, 41
Bond, J. R., et al. 2000, in Proc. IAU Symposium 201, PASP, in press (astro-ph/0011378)
Bryan, G.L. & Norman, M.L. 1998, ApJ, 495, 80
Burles, S., & Tytler, D. 1998, ApJ, 499, 699
Caldwell, R.R., Dave, R. & Steinhardt, P.J. 1998, Ap&SS, 261, 303
Carlstrom, J.E., Joy, M.K., Grego, L., Holder, G.P., Holzapfel, W.L., Mohr, J.J., Patel, S. & Reese, E.D. 1999, *Physica Scripta*, 60, in press (astro-ph/9905255)
Carroll, S., Press, W. & Turner, E. 1992, ARA&A, 30, 499
Chartas, G., Garmire, G., Nousek, J., Koch, S., Kissel, S., Prigozhin, G., & Bautz, M. 1998, SPIE Proceedings, 3444, 258
Eisenstein, D.J. 1996, PhD dissertation, Harvard University
Eisenstein, D.J. & Hu, W. 1998, ApJ, 504, L57
Evrard, A.E., Metzler, C.A. & Navarro, J.F. 1996, ApJ, 469, 494
Freese, K., Adams, F. C., & Frieman, J. A. 1987, Nucl. Phys. B, 287, 797
Friedrich, P., Brauninger, H., Burkert, W., Dohring, T., Egger, R., Hasinger, G., Oppitz, A., Predehl, P. & Trumper, J. 1998, SPIE Proceedings, 3444, 369
Gioia, I.M., Maccacaro, T., Schild, R.E., Wolter, A., Stocke, J.T., Morris, S.L. & Henry, J.P. 1990, ApJS, 72, 567
Gross, M.A.K., Zomerville, R.S., Primack, J.R., Holtzman, J. & Klypin, A. 1998, MNRAS, 301, 81
Holder, G.P., Mohr, J.J., Carlstrom, J.E., Evrard, A.E. & Leitch, E.M. 2000, ApJ, submitted (astro-ph/9912364)
Huey, G., Wang, L., Dave, R., Caldwell, R. R., & Steinhardt, P. J. 1999, Phys. Rev. D, 59
Jenkins, A. et al. 2000, MNRAS, submitted, astro-ph/0005260
Lacey, C. & Cole, S. 1994, MNRAS, 271, 676
Lange, A. E., et al. 2000, Phys. Rev. D, submitted, astro-ph/0005004
Lee, J. & Shandarin, S.F. 1999, ApJ, 517, L5
Metzler, C. A. 1998, ApJ, submitted, (astro-ph/9812295)
Mohr, J.J. & Evrard, A.E. 1997, ApJ, 491, 13
Mohr, J.J., Mathiesen, B. & Evrard, A.E. 1999, ApJ, 517, 627
Mohr, J.J., Carlstrom, J.E., Holder, G.P., Holzapfel, W.L., Joy, M.K., Leitch, E.M. & Reese, E.D. 1999, Proceedings of the VLT Opening Symposium, Antofagasto, Chile, in press (astro-ph/9905256)
Mushotzky, R.F. & Scharf, C.A. 1997, ApJ, 482, 13
Navarro, J. F., Frenk, C. S., & White, S. D. M. 1997, ApJ, 490, 493 (NFW)
Peebles, P.J.E., 1980, *The Large Scale Structure of the Universe*, Princeton University Press: Princeton
Pen, U.-L. 1998, ApJ, 498, 60
Perlmutter, S., Turner, M. S., & White, M. 1999, Phys. Rev. Lett., 83, 670
Perlmutter, S. et al. 1999, ApJ, 517, 565
Press, W.H. & Schechter, P. 1974, ApJ, 193, 437
Press, W.H., Teukolsky, S.A., Vetterling, W.T. & Flannery, B.P., 1992, *Numerical Recipes in C: The Art of Scientific Computing*, 2nd Edition, Cambridge University Press: Cambridge
Ratra, B., & Peebles, P. J. E. 1988, Phys. Rev. D, 37, 3406
Raymond, J.C. & Smith, B.W. 1977, ApJS, 35, 419
Romer, A.K., Viana, P.T.P., Liddle, A.R. & Mann, R.G. 2000, ApJ, submitted (astro-ph/9911499)
Schmidt, B.P. et al. 1998, ApJ, 507, 46
Turner, M. S., & White, M. 1997, Phys. Rev. D, 56, 4439
Viana, P.T.P. & Liddle, A.R. 1996, MNRAS, 281, 323
Viana, P.T.P. & Liddle, A.R. 1999, MNRAS, 303, 535
Vikhlinin, A., McNamara, B.R., Forman, W., Jones, C., Quintana, H. & Hornstrup, A. 1998, ApJ, 503, 77
Wang, L., & Steinhardt, P. J. 1998, ApJ, 508, 483
Wang, L., Calwell, R. R., Ostriker, J. P., & Steinhardt, P. J. 2000, ApJ, in press, (astro-ph/9901388)
White, S.D.M., Efstathiou, G., Frenk, C.S. 1993, MNRAS, 262, 1023
White, M. 1998, ApJ, 506, 495
White, M., Scott, D., & Pierpaoli, E. 2000, ApJ, in press, astro-ph/0004385